Monthly Notices
of the
ROYAL ASTRONOMICAL SOCIETY

MNRAS **460,** 1716–1724 (2016)
Advance Access publication 2016 May 6

doi:10.1093/mnras/stw1070

The mass and spin of the extreme Narrow Line Seyfert 1 Galaxy 1H 0707−495 and its implications for the trigger for relativistic jets

Chris Done[1]★ and Chichuan Jin[2]

[1]*Centre for Extragalactic Astronomy, Department of Physics, University of Durham, South Road, Durham DH1 3LE, UK*
[2]*Max-Planck-Institut für Extraterrestrische Physik, Giessenbachstrasse, D-85748 Garching, Germany*

Accepted 2016 May 3. Received 2016 April 12; in original form 2015 June 15

ABSTRACT

Relativistic reflection models of the X-ray spectrum of the 'complex' Narrow Line Seyfert 1 (NLS1) 1H 0707−495 require a high-spin, moderate-inclination, low-mass black hole. With these parameters fixed, the observed optical/UV emission directly determines the mass accretion rate through the outer disc and hence predicts the bolometric luminosity. This is 140–260 times the Eddington limit. Such a disc should power a strong wind, and winds are generically expected to be clumpy. Changing inclination angle with respect to a clumpy wind structure gives a possible explanation for the otherwise puzzling difference between 'complex' NLS1 such as 1H 0707−495 and 'simple' ones like PG 1244+026. Lines of sight which intercept the wind show deep absorption features at iron from the hot phase of the wind, together with stochastic dips and complex absorption when the clumps occult the X-ray source (complex NLS1), whereas both these features are absent for more face-on inclination (simple NLS1). This geometry is quite different from the clean view of a flat disc which is assumed for the spin measurements in relativistic reflection models, so it is possible that even 1H 0707−495 has low spin. If so, this re-opens the simplest and hence very attractive possibility that high black hole spin is a necessary and sufficient condition to trigger highly relativistic (bulk Lorentz factor ∼10–15) jets.

Key words: accretion, accretion discs – black hole physics.

1 INTRODUCTION

There are a lot of different types of active galactic nuclei (AGN), yet there are only a limited number of fundamental parameters which can determine their behaviours. There is black hole mass, mass accretion rate and spin, with inclination, abundances and environment as further factors which can affect how the AGN is seen as well as non-deterministic factors such as the history of the accretion flow (hysteresis and/or magnetic flux accumulation).

Black hole mass can now be estimated e.g. through scaling relations using the full width at half-maximum of the Hβ line together with optical luminosity. A thin disc model fit to the optical/UV data then directly gives the absolute accretion rate, $\dot{M}$, through the outer disc for a given inclination angle (Laor & Davis 2011). Emission from the inner disc does not affect this as smaller radii emit at higher temperatures, and so contribute to the far-UV rather than to the optical for typical AGN parameters. Thus simply observing the optical emission from the outer disc is sufficient to set the absolute mass accretion rate of the entire flow in standard disc models.

The inner disc properties instead determine the total bolometric luminosity as spin sets the inner edge of the disc, and hence the total efficiency. High prograde spin leads to additional luminosity at higher temperatures from the same mass accretion rate through the outer disc compared to a lower spin. If the mass, inclination and spin are known, then the absolute $\dot{M}$ through the outer disc directly predicts the total bolometric luminosity, and hence $L_{\rm bol}/L_{\rm Edd}$ of the accretion flow.

Laor & Davis (2011) used this argument in reverse. They measured $\dot{M}$ from the optical/UV flux, then integrated the observed spectral energy distribution (SED) to estimate $L_{\rm bol}$ and hence constrained spin in their sample of AGN. However, there are other ways to constrain spin. First, via the peak temperature and luminosity of the disc continuum as discussed above. This disc continuum fitting technique can be used to good effect in black hole binaries, where the disc peaks at X-ray temperatures (e.g. Ebisawa, Mitsuda & Hanawa 1991; Kubota, Makishima & Ebisawa 2001; Done, Gierliński & Kubota 2007). However, in AGN the disc typically is expected to peak in the far-UV, which is unobservable due to interstellar absorption. Instead, the iron line profile can be used to constrain spin. X-ray illumination of the disc produces a fluorescence iron Kα line, whose profile contains the imprint of the (spin-dependent) innermost disc radius as well as the illumination pattern and inclination

★ E-mail: chris.done@durham.ac.uk

(Fabian et al. 1989, 2000). The new reverberation technique uses this together with the light travel time delays (Fabian et al. 2009) to map the reflecting structures (see e.g. the review by Uttley et al. 2014).

Multiple AGN now have high spin as determined by the iron line profile (see e.g. the compilation of Reynolds 2013). The most convincing of these have reverberation mapping as well, and tend to be Narrow Line Seyfert 1s (NLS1) such as 1H 0707−495 (Fabian et al. 2009). The iron line profile also gives inclination, so for these systems the optical/UV continuum gives absolute $\dot{M}$, which, combined with the known spin, gives $L_{\rm bol}$ and hence $L_{\rm bol}/L_{\rm Edd}$.

Here we use this technique on two specific, well-studied NLS1, PG 1244+026 (hereafter PG1244) and 1H0707−495 (hereafter 1H0707). These have very similar Hβ linewidths, and very similar optical/UV continua so they form a well-matched pair in mass and absolute mass accretion rate. Both also have high spin as determined from the iron line/reverberation techniques, though it is clear that this is a much stronger constraint in 1H0707 (Fabian et al. 2009; Zoghbi et al. 2010; Kara et al. 2013) than in PG1244 (Kara et al. 2014). We derive $L_{\rm bol}/L_{\rm Edd}$ from the outer disc mass accretion rate and find that both are highly super-Eddington. The disc is unlikely to remain flat under such conditions, with numerical simulations showing that such flows should power a strong, clumpy wind from the inner disc (Takeuchi, Ohsuga & Mineshige 2014). Inclination with respect to this wind should then be an important additional parameter determining the observational appearance of the inner flow. This is interesting, as while PG1244 and 1H0707 are very similar as regards their optical/UV emission, they have very different X-ray properties. 1H0707 shows deep X-ray dips, with extremely strong Fe Kα features in these low flux episodes, whereas the dips (and associated extreme iron features) are absent in PG1244. This difference in X-ray behaviour was classified as 'complex' and 'simple', respectively (Gallo 2006). Reverberation lags are typically very short in the complex NLS1 (30 s for 1H0707; Fabian et al. 2009) and longer in the simple ones (200 s for PG1244; Alston, Done & Vaughan 2014).

We propose that inclination with respect to a strong wind from a super-Eddington accretion flow is the major underlying difference between these two different types of NLS1. Absorption in a highly ionized wind can fit the observed iron features seen in the non-dip spectra of 1H0707, while stochastic occultations by cooler clumps in the wind can produce the dips and give rise to more complex spectral curvature (Hagino et al. 2016, see also Miller et al. 2007, 2010; Mizumoto, Ebisawa & Sameshima 2014). These dips also shorten the reverberation time lags, so that the observed 30 s reverberation delay seen in 1H0707 can be produced from an intrinsic lag of 200–300 s, as seen in PG1244 (Gardner & Done 2015). More face-on inclination angles do not intercept (much of) the wind, and so do not show the extreme features at iron, nor the dips.

This is very different from the standard 'lamppost' model used to derive the high black hole spin in these objects, where an extremely compact X-ray source on the spin axis of the black hole illuminates a flat disc (Miniutti & Fabian 2004). In this geometry, the dips are caused by an extremely compact X-ray source on the spin axis of the black hole approaching the event horizon. The resulting strong light bending focuses the intrinsic continuum away from the observer (producing the drop in flux) so it instead strongly illuminates the very inner disc, producing a very centrally concentrated emissivity for the line which can simultaneously explain the very strongly relativistically smeared, reflection-dominated emission seen in the dips (Miniutti & Fabian 2004). However, if the lamppost geometry is not correct, the spins derived from it need not be correct either. This could remove the requirement that there are high-spin *radio-quiet* objects, re-opening the possibility of the spin-jet paradigm where high spin is a necessary and sufficient trigger for highly relativistic jets.

2 CONSTRAINTS FROM RELATIVISTIC REFLECTION MODELS

The classic way to measure black hole spin is via the iron line Kα profile in the 2–10 keV bandpass (Fabian et al. 1989, 2000). 1H0707 always shows strong broad features at 6–7 keV, especially during the deep X-ray intensity dips. Fitting reflection models to these spectra gives a spin measurement which is always high (e.g. Fabian et al. 2004, 2009, 2012). The most complete models of Zoghbi et al. (2010) give a disc inner radius of $r_{\rm in} = 1.23^{+0.07}_{-0.0} R_{\rm g}$ (corresponding to spin $a_* = 0.998^{+0.0}_{-0.001}$) for a disc inclination of $58.5^{+0.8}_{-0.7}$ and emissivity index of $6.6^{+1.9}_{-1.1}$. While these can all be explained within the lamppost model, the data additionally require that iron is overabundant by a factor of ∼9 in order to match the observed features.

Fitting the lag-frequency and lag-energy data from reverberation mapping also gives constraints on the black hole mass, spin and disc inclination, though there are significant degeneracies between these parameters from the spectral-timing data alone (e.g. Cackett et al. 2014). Assuming that the lag time-scale $\Delta t \sim 2H/c = 2hR_{\rm g}/c$, where H is the physical height of the lamppost and $h = H/R_{\rm g}$ is this in terms of gravitational radii, only constrains the product hM rather than each parameter separately. In 1H0707, the observed 30 s soft lag (Fabian et al. 2009; Zoghbi et al. 2010; Zoghbi, Uttley & Fabian 2011) corresponds to an intrinsic 80 s light travel time after correcting for spectral dilution, which implies a lamppost height of $4R_{\rm g}$ for a 2×10^6 M$_\odot$ black hole (Kara et al. 2013). However, the spectral data discussed above strongly require that the lamppost height is small from the strongly centrally peaked emissivity (e.g. Fabian et al. 2012). Hence for these data a lamppost height of $2R_{\rm g}$ implies a black hole mass of 4×10^6 M$_\odot$, though at such low heights relativistic effects become very important. Light bending will increase the proper path length, and time dilation (Shapiro delay) will increase the time difference. A lamppost source at height $2R_{\rm g}$ above a flat disc around a maximally spinning black hole has a minimum lag time of $2.6 - 1.235R_{\rm g}/c$ (face on–edge on) if light travels in straight lines without time dilation. Including all relativistic effects lengthens these to around $4R_{\rm g}/c$ (Dovciak, private communication; see also Dovciak et al. 2014). Thus a lamppost height of $2R_{\rm g}$ still implies a 2×10^6 M$_\odot$ black hole.

In sharp contrast, the simple NLS1 PG1244 has no deep intensity dips, so the iron features are not so strong and do not of themselves require high spin (Jin et al. 2013, hereafter J13), nor very strong iron overabundance (J13 assume solar, Kara et al. 2013 find iron is $2.1^{+0.4}_{-0.1}\times$ solar). However, interpreting a (rather low significance: see Alston et al. 2014) lag of 1000 s at the iron line energy in a reflection dominated scenario gives $r_{\rm in} = 1.6^{+0.5}_{-0.3} R_{\rm g}$ (corresponding to spin $a_* = 0.97^{+0.03}_{-0.29}$) and inclination of $38^\circ \pm 3^\circ$ for a lamppost height of $5R_{\rm g}$ above a 1.3×10^7 M$_\odot$ black hole (Kara et al. 2014).

3 ZEROTH ORDER ESTIMATES OF MASS AND MASS ACCRETION RATE FROM THE OPTICAL SPECTRUM

Fig. 1 shows the optical spectrum of 1H0707 from Cerro Tololo Inter-American Observatory (CTIO) (black; Leighly & Moore 2004) together with that of PG1244 from Sloan Digital Sky

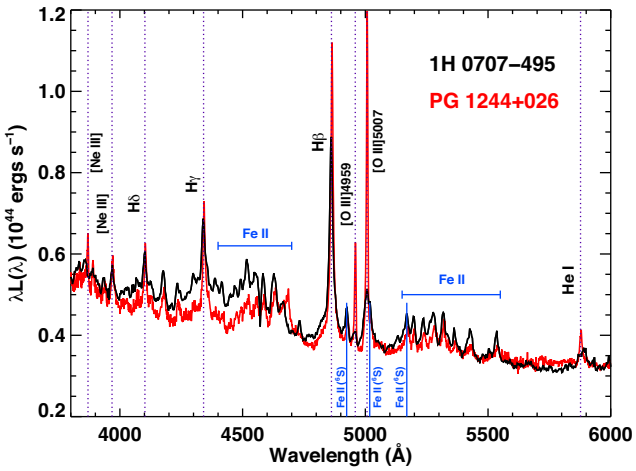

Figure 1. The optical spectra from 1H0707 (black; Leighly & Moore 2004) and PG1244 (SDSS, red, rescaled by 0.84 to match 1H0707). The overall luminosities are similar, as are the lines (e.g. Fe II and broad lines), except that 1H0707 has much weaker forbidden lines and narrow lines (e.g. [O III]).

Survey (SDSS). These are redshift corrected using $z = 0.0398$ and 0.0482, de-reddened with $E(B-V) = 0.073$ and 0.032 (Bessell 1991; Kalberla et al. 2005), and fluxed with distances of 168.6 and 206.2 Mpc, respectively. Note that the redshift of 1H0707 used here is slightly different from that of 0.040568 ± 0.000150 quoted in the NASA/IPAC Extragalactic Database (NED) from the 6dF survey (Jones et al. 2009), as this redshift gave a noticeable offset with respect to the Fe II lines in PG1244. The 6dF redshift was calculated from cross-correlation with a late-type galaxy template, using the absorption lines. However, Leighly & Moore (2004) detect no absorption lines from the host galaxy in their spectrum, and instead determined a redshift of ∼0.04 (no uncertainty given) from the broad Mg II and Hβ emission lines. We determine our redshift by cross-correlating the spectrum of 1H0707 with that of PG1244 in the 4000–6700 Å region, after blacking out the regions where strong narrow lines dominate in PG1244 but not in 1H0707. This gives $z = 0.03979 \pm 0.00084$ factoring in the uncertainty on the PG1244 redshift from SDSS. We use this slightly lower value as we are most interested in a comparison of 1H0707 with PG1244, but the change in implied distance is less than 2 per cent so this has no significant impact on the luminosity. We rescale PG1244 by a factor of 0.84 so as to overlay it on top of 1H0707. Hence, the two objects have the same optical luminosity to within 20 per cent.

Fig. 1 shows that 1H0707 has much weaker narrow emission lines than PG1244, but that the broad emission lines are extremely similar, especially the strength of the Fe II emission line blends and the ratio of Fe II to the broad Hβ (PG1244 has a narrow Hβ line component which makes it appear stronger.). The Fe II emission is clearly not a factor of ∼5 larger in 1H0707 than in PG1244, so this does not support the difference in iron abundance suggested by the relativistic reflection fits (Section 2), though we note that the Fe II strength depends also on $L/L_{\rm Edd}$ as well as abundance (Ferland et al. 2009). This is discussed further in Section 5.2.

The Hβ linewidth is determined as in Jin et al. (2012a), i.e. after subtraction of the strong Fe II lines, and subtraction of a narrow component of Hβ with width fixed to that of the [O III] lines. This gives very similar Hβ full width at half-maximum of 980 and 940 km s^{-1}, and $\lambda L_{5100} = 3.3$ and 3.9×10^{43} erg s^{-1} for 1H0707 and PG1244, respectively. Thus, they have very similar mass estimates from Hβ, with $M \sim 4 \times 10^6\,{\rm M}_\odot$ or $M \sim 2 \times 10^6\,{\rm M}_\odot$ depending on whether the scaling relations of Vestergaard & Peterson (2006) or Woo & Urry (2002) are used. The similarity in linewidths does not at all support the factor of nearly 10 difference in mass from the reverberation results.

The bolometric luminosity is typically estimated as $9 \times \lambda L_{5100}$ (e.g. Kaspi et al. 2000), so both these sources have $L_{\rm bol} \sim 3 \times 10^{44}$ erg cm^2 s^{-1}. This is close to the Eddington limit, $L_{\rm Edd} = 2.6(5.2) \times 10^{44}$ erg s^{-1}, for a black hole mass of $2(4) \times 10^6\,{\rm M}_\odot$. However, bolometric correction $\kappa_{5100} = L_{\rm bol}/\lambda L_{5100}$ clearly changes with mass and mass accretion rate. Several studies have shown that the 'standard' value of $9\lambda L_{5100}$ used above is only appropriate for the broad line Seyferts ($L/L_{\rm Edd} < 0.2$), while objects around $L_{\rm Edd}$ require correction factors of 20–40 (Vasudevan & Fabian 2007, 2009; Jin et al. 2012a; Jin, Ward & Done 2012b). This would put both 1H0707 and PG1244 at $L_{\rm bol} \sim 10^{45}$ erg s^{-1}, strongly super-Eddington for either black hole mass.

At such high Eddington fractions it is clearly debatable as to whether the Hβ scaling relations hold. Marconi et al. (2008) suggest a correction to the mass scalings such that the broad line region (BLR) clouds trace the effective gravity. Using this, the black hole masses increase to around $10^7\,{\rm M}_\odot$, with $L_{\rm Edd} = 1.3 \times 10^{45}$ erg s^{-1}, so the accretion flow is still close to the Eddington limit as required for the higher bolometric correction.

The radiation pressure correction to the mass is not widely used as the general lack of observed wind features for the low ionization BLR lines form a strong argument against such effects being important (Baskin, Laor & Stern 2014a). Physically, this could indicate that the clouds are optically thick to electron scattering, with columns of $>10^{24}$ cm^{-2} (consistent with the low ionization broad lines forming in the disc: Collin-Souffrin et al. 1980), or that the radiative acceleration only affects the front face of the cloud (Baskin, Laor & Stern 2014b). However, part of the Hβ line is clearly blueshifted (Fig. 1), indicating that these objects could be so extreme that even part of the low ionization lines (as well as the high ionization lines such as C IV) come predominantly from a wind (see also Leighly & Moore 2004; Leighly 2004).

The new results from reverberation mapping (see Section 2) strongly require that the radiation pressure corrected mass is not appropriate, and that the mass for 1H0707 is $\leq 4 \times 10^6\,{\rm M}_\odot$. The similarity of the Hβ emission linewidths supports a similarly low mass for PG1244.

4 BROADBAND SPECTRA: MASS ACCRETION RATE AND INCLINATION

We assemble simultaneous optical/UV/X-ray SED from *XMM–Newton* data, using the optical monitor (OM) to give optical and UV photometric points along with the X-ray data from the EPIC pn camera. All *XMM–Newton* data reduction and spectra extraction were performed following the standard procedures with SAS v14.0.0 and the latest calibration files. For both 1H0707 and PG1244, we extend the SED down to lower energies using continuum points from the optical spectra discussed above. While these data are not simultaneous, the spectra match extremely well for PG1244, whereas for 1H0707 the optical spectrum discussed in Section 2 is 40 per cent lower than the OM data. This is probably due to long-term variability, but the CTIO spectrum was not fluxed (Leighly, private communication), so part of this may also be due to slit losses.

NLS1 in general are less optically variable than broad line Seyferts (e.g. Ai et al. 2013, but see Kelly et al. 2013), despite having higher X-ray variability (e.g. Leighly 1999; Ponti et al. 2012). 1H0707 has no optical monitoring data, but UV monitoring by the

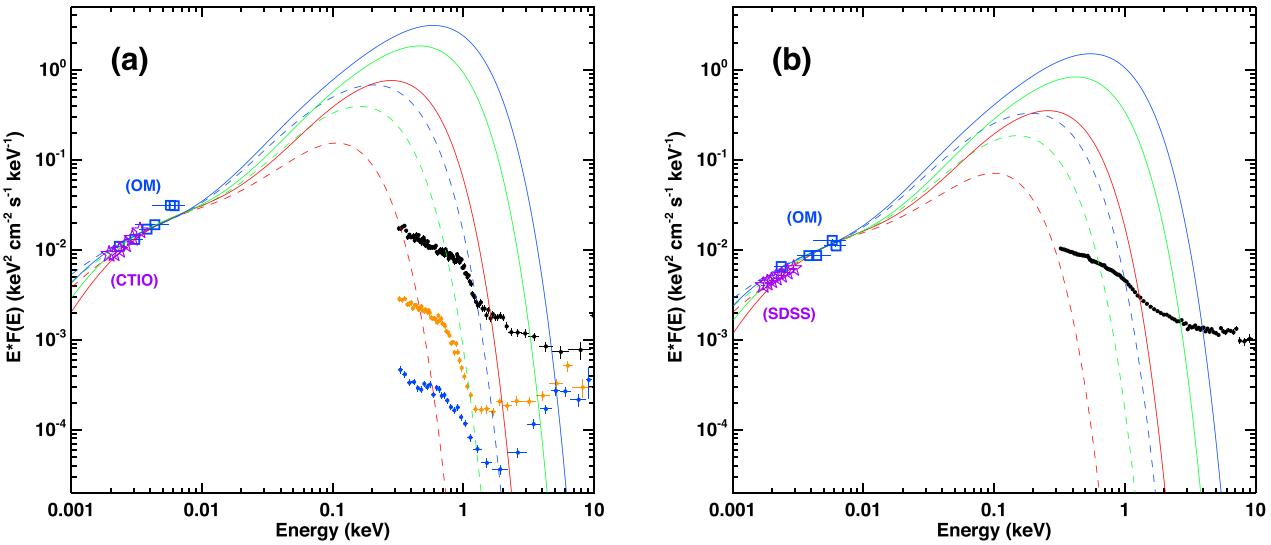

Figure 2. Continuum fitting with OPTXCONV to the NLS1 (a) 1H 0707−495 and (b) PG 1244+026. The red, green and blue solid lines show the disc emission inferred for an inclination of 30° from the optical/UV continuum for spin of $a = 0$, 0.9 and 0.998, respectively, for a mass of $2 \times 10^6\,M_\odot$, while the dashed lines show the same for a mass of $10^7\,M_\odot$. For 1H 0707−495, the optical continual points (star symbol) extracted from the CTIO spectrum were scaled up by 50 per cent to account for the discrepancy with OM data due to long-term variability and/or aperture difference.

XMM–Newton OM (UVW1 filter) shows a factor of 30 per cent variability on time-scales of years but less than 2 per cent variability within a single observation of ≤100 ks time-scale (Robertson et al. 2015; see also Smith & Vaughan 2007 for similar limits on fast variability in UVW2).

By contrast, 1H0707 shows dramatic X-ray variability. The source flux can drop by a factor of ∼30, accompanied by strong variation in spectral shape (e.g. Zoghbi et al. 2010). We systematically searched all available *XMM–Newton* observations for data which spanned the range in X-ray shape and intensity. We extracted pn spectra from every 10 ks segment of each observation, and selected the highest spectrum (Fig. 2a: black spectrum from the 60–70 ks segment in the observation on 2010-09-15, OBSID: 0653510401). The lowest spectrum has a low count rate, so we combine two very similar spectra from 40–50 ks and 50–60 ks segments in the observation on 2011-01-12 (OBSID: 0554710801) to obtain a low-state spectrum with better signal-to-noise ratio (Fig. 2a: blue spectrum). We also select an intermediate state (Fig. 2a: orange spectrum) from the 10–20 ks segment in the observation on 2007-05-14 (OBSID: 0506200301). The OM data for these observations are remarkably constant. The largest difference is 10 per cent in the UVW2 flux between 2007-05-14 (intermediate-state X-ray spectrum) and 2010-09-15 (high-state X-ray spectrum), the other differences in the same OM filters are all less than 4 per cent. Since only the 2010-09-15 observation has exposures in six OM filters (i.e. UVW2, UVM2, UVW1, U, B, V), we used this data set in Fig. 2(a). A similar range in X-ray spectra is shown by Vasudevan et al. (2011), and they also find that this is not accompanied by strong optical/UV variability.

For PG1244, a 6 month optical reverberation mapping campaign failed to constrain the black hole mass as there was no significant variability (K. Denny, private communication). We extracted the two archival IUE observations of PG1244, taken 10 years apart, and these show variability by a factor of ∼2, similar to the variability seen between the OM and *GALEX* UV photometry (J13). Similarly, the 2–10 keV band in PG1244 varies by a factor of 2 on both long and short time-scales (J13 and the compilation of Ponti et al. 2012). The spectral shape remains more or less constant during this variability, so we use pn data from the longest *XMM–Newton* observation (123 ks *XMM–Newton* on 2011-12-25, OBSID: 0675320101) to define the typical source spectrum (J13; Done et al. 2013, hereafter D13). We use the simultaneous OM data from this observation which matches well to the SDSS spectrum.

Figs 2(a) and (b) show the resulting SEDs for 1H0707 and PG1244, respectively, where we de-absorb the X-rays using only the Galactic gas column of $N_{\rm H} = 4.31$ and 1.87×10^{20} cm^{-2} (Kalberla et al. 2005), and de-redden the corresponding optical/UV values of $E(B-V) = 0.073$ and 0.032 (Bessell 1991). The resultant SEDs are then de-redshifted to the AGN rest frame. These are the lowest possible absorption values as they only include material in our galaxy. Any additional material in the host galaxy will increase the intrinsic UV/soft X-ray flux, and hence increase the inferred mass accretion rate.

The optical/UV emission looks like a disc spectrum in both objects, with no obvious flattening at red wavelengths which would indicate substantial host galaxy contamination (see e.g. the spectrum of IRAS 13224−3809 in fig. 1 of Leighly & Moore 2004). Similarly, there are no obvious absorption lines from the host galaxy in the spectra of either object, again indicating that any host galaxy contamination is low. Hence we fit with a disc model to estimate the mass accretion rate. We use the OPTXCONV model of D13, as this approximates the full radiative transfer, fully relativistic models of Hubeny et al. (2001) (updated in Davis, Woo & Blaes 2007), but is more flexible in spectral fitting as it is analytic rather than limited to precomputed tables. The intrinsic disc spectrum is calculated using a colour–temperature correction factor, $f_{\rm col}$, to approximate the effect of electron scattering in the disc photosphere. This colour temperature correction factor is not a constant in these models, but is dependent on the photosphere temperature. At small radii, the effective temperature is in the far-UV/soft X-ray, where the true absorption opacity is very low. The photosphere is set by the point at which the effective optical depth, $\tau_{\rm eff} \approx \sqrt{\tau_{\rm es}\tau_{\rm abs}}$ is unity, where $\tau_{\rm es}$, $\tau_{\rm abs}$ are the electron scattering and true absorption optical depth, respectively. Photons can escape after multiple scatterings from deep inside the disc where the temperature is higher giving rise

Table 1. Comparison of the OPTXCONV results including the self-consistent colour–temperature correction with those from KERRBB with $f_{\rm col} = 1$. Both disc models give similar (within a factor of ∼2 in $\dot{m}$ from the optical/UV continuum) fits as both have $f_{\rm col} = 1$ in the optical region. The X-ray excess is defined as the disc model flux in the 0.3–2 keV bandpass, absorbed by the Galactic column, divided by the observed flux of 1.39×10^{-11} erg cm^{-2} s^{-1} (the maximum) for 1H0707, and 1.33×10^{-11} erg cm^{-2} s^{-1} for PG1244. The OPTXCONV models extend further into the soft X-ray bandpass due to their $f_{\rm col} \sim 2$ in the EUV region, so require larger losses.

SOURCE	M	i	Spin	$\dot{m}$ (optx)	X-ray excess (optx)	$\dot{m}$ (kerrbb)	X-ray excess (kerrbb)
1H0707	2×10^6	30	0	20	36	14	2.1
1H0707	2×10^6	30	0.9	59	162	35	27
1H0707	2×10^6	30	0.998	146	360	63	61
1H0707	10^7	30	0	0.9	0.24	0.6	0.0
1H0707	10^7	30	0.9	2.5	4.9	1.5	0.02
1H0707	10^7	30	0.998	6.3	19	2.7	0.20
1H0707	2×10^6	60	0	44	90	31	11
1H0707	2×10^6	60	0.9	121	390	79	140
1H0707	2×10^6	60	0.998	265	755	142	350
1H0707	10^7	60	0	1.9	1.9	1.4	0.002
1H0707	10^7	60	0.9	5.1	28	3.4	1.5
1H0707	10^7	60	0.998	11	92	6.0	10
PG1244	2×10^6	30	0	13	18	9.3	1.0
PG1244	2×10^6	30	0.9	38	80	23	14
PG1244	2×10^6	30	0.998	94	175	42	31
PG1244	10^7	30	0	0.6	0.1	0.4	0.0
PG1244	10^7	30	0.9	1.7	2.3	1.0	0.01
PG1244	10^7	30	0.998	4.1	9.0	1.8	0.07

to a spectrum which is approximately $B_\nu(f_{\rm col}T)/f_{\rm col}^4$ with $f_{\rm col} \sim 2$. Conversely, in the outer regions of the disc, where the temperature is in the optical, the true absorption opacity is high so $f_{\rm col} \sim 1$. This change in colour temperature between the optical and far-UV predicts a change in curvature of the disc spectrum in the UV (Done et al. 2012), and this intrinsic spectrum then has relativistic effects superimposed to give the observed emission (D13).

At a fixed energy, $h\nu << kT_{\rm peak}$ where $T_{\rm peak}$ is the temperature at which the disc luminosity peaks, a standard Shakura–Sunyaev disc has $L_\nu \propto (M\dot{M})^{2/3} \cos i$ (e.g. Davis & Laor 2011). This uses only the optical/UV flux to determine the mass accretion rate through the outer disc. However, standard discs have constant mass accretion rate with radius, so this also sets the total $L_{\rm bol} = \eta \dot{M} c^2$. Hence $\dot{m} = \dot{M}/\dot{M}_{\rm Edd} \propto \eta L_\nu^{3/2}/(M^2 \cos^{3/2} i)$ where $\eta \dot{M}_{\rm Edd} c^2 = L_{\rm Edd} \propto M$ and the efficiency $\eta = 0.0572$, 0.155 and 0.321 for $a_* = 0, 0.9$ and 0.998 as the innermost stable circular orbit decreases from $r_{\rm isco} = 6$, 2.32 to 1.236. Hence the observed optical/UV continuum determines $\dot{m}$ from the combination of $\eta/(M^2 \cos^{3/2} i)$, and this is maximized for the smallest mass, highest spin, highest inclination. The analytic approximation gives a nice way to see the effect of all the parameters, and indeed in the figures below it is clear that even the further UV data point is still on the Rayleigh–Jeans tail of the disc spectrum so that the approximations should be valid, but we stress that we use full spectral fitting to derive all mass accretion rates given below.

For 1H0707 solid red, green and blue lines in Fig. 2(a) show the results assuming a black hole mass of 2×10^6 M$_\odot$, for a spin of 0 (red), 0.9 (green) and 0.998 (blue) assuming a standard AGN inclination of 30°. The derived mass accretion rate through the outer disc is $\dot{m} = 20$, 63 and 151, respectively, with increasing luminosity and peak temperature with black hole spin as expected from the discussion above. Even for the higher mass of 10^7 M$_\odot$, derived from applying the radiation pressure correction to the Hβ linewidth, gives $\dot{m} = 0.9$, 2.7 and 6.6, respectively, though the bolometric luminosity and peak temperature are now both lower by a factor of ∼5 and 3, respectively, for each spin.

Fig. 2(b) shows the same sequence of models for PG1244 for $i = 30°$. The derived mass accretion rate is slightly lower, with $\dot{m} = 14$, 43 and 110 for a mass of 2×10^6 M$_\odot$, compared to $\dot{m} = 0.6$, 1.9 and 4.8 for 10^7 M$_\odot$.

For 1H0707 we also explore the effect of a higher inclination, as required by the relativistic reflection fits (Section 2). This gives $\dot{m} = 44$, 120 and 269 for the mass of 2×10^6 or $\dot{m} = 1.9$, 5.0 and 11 for 10^7 M$_\odot$ for an inclination of 60°. The fits are all summarized in Table 1. It is clear that only the very highest mass, lowest spin and lowest inclination solutions have sub-Eddington accretion flows. This is exactly the opposite requirement to the relativistic reflection fits in 1H0707, which need low mass, high spin and high inclination (Section 2).

This conclusion does not strongly depend on the colour–temperature correction in OPTXCONV as this is close to unity in the optical, reaching a maximum of around 1.2 for the highest temperatures which contribute to the UV data used here. This decreases the UV flux slightly, as it pushes it to higher energies [see e.g. fig. 1(a) in Done et al. 2012]. Thus the observed UV flux can be fitted with a slightly lower mass accretion rate if there is no colour–temperature correction. However, this is in general a rather small effect. We demonstrate this explicitly by repeating the fits with the KERRBB disc model, fixing $f_{\rm col} = 1$. The inferred mass accretion rates are around a factor of 2 smaller for the same mass/spin, but all the fits with high spin are still highly super-Eddington (see Table 1).

However, the colour–temperature correction does have a large effect on the predicted soft X-ray extent of the disc emission as the peak disc temperature is boosted by a factor of ∼2 by this effect [see e.g. fig. 1(a) in Done et al. 2012]. The peak disc temperature is $T_{\rm peak} \propto f_{\rm col}[(\dot{M}M)/R_{\rm isco}^3]^{1/4} \propto f_{\rm col}[(L_\nu/\cos i)^{3/2}/(M^3 r_{\rm isco}^3)]^{1/4}$ so

it is highest for the lowest mass, highest spin, highest inclination solutions with highest colour temperature. Figs 2(a) and (b) show the high-energy extrapolation of the OPTXCONV model SED fits to the optical/UV. It is clear that all these dramatically over-predict the soft X-ray flux except for the lowest spin, highest mass black hole models. We quantify this by integrating the disc model flux in the 0.3–2 keV bandpass, including the effect of Galactic absorption, and divide this by the observed 0.3–2 keV flux. For PG1244 we use the average flux of 0.3–2 keV flux of 1.33×10^{-11} erg cm^{-2} s^{-1}, while for 1H0707 we pick the maximum observed flux of 1.39×10^{-11} erg cm^{-2} s^{-1}. These ratios are typically much larger than unity for all except the highest mass, lowest spin, lowest inclination models for the colour–temperature corrected models, while they are substantially reduced by removing the colour–temperature correction factor (see Table 1). However, even without a colour–temperature correction, all high-spin, high-inclination solutions for 1H0707 all dramatically over-predict the soft X-ray flux.

5 DISCUSSION

1H0707 is the most convincing candidate for extremely high black hole spin as derived from the reflection/reverberation fits to the X-ray spectral-timing properties. However, these fits require a low-mass, high-spin black hole, viewed at high inclination, i.e. exactly the case where the optical/UV fits imply the most strongly super-Eddington flows. This means that the inner disc is highly unlikely to be flat. Since a flat disc was assumed in the lamppost geometry to derive these constraints on mass, spin and inclination, clearly these need not be robust. We critically examine these below.

5.1 Alternative models for the X-ray spectra and variability of 1H0707?

The dramatic X-ray spectral features in 1H0707 are so broad and strong around iron that probably all relativistic reflection models will require high spin, irrespective of the specific reflector geometry. However, it is possible to fit the spectral features with a very different model, based on absorption in a clumpy wind (Hagino et al. 2016). This is shown schematically in Fig. 3. Winds are generically expected to be clumpy, and the super-Eddington wind simulations of Takeuchi et al. (2014) show clumps forming from the (almost) standard Rayleigh–Taylor instability. However, the material is also illuminated by X-rays and in pressure balance, so there is an ionization instability which produces two distinct phases in the gas, resulting in clumps of cooler, less ionized material embedded in less dense, highly ionized gas (Krolik, McKee & Tarter 1981).

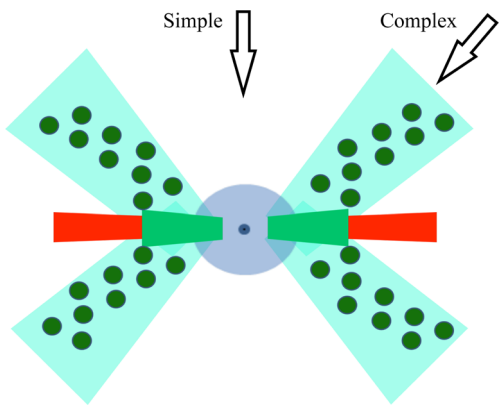

Figure 3. A schematic picture of the clumpy wind geometry from a super-Eddington flow which could explain the difference in X-ray properties between simple and complex NLS1. The hard X-ray corona (inner blue flow) is absorbed by the wind at high inclinations, with the smooth, highly ionized absorption (cyan) producing a strong drop at the (blue-shifted) line energy, while cooler, less ionized clumps (green) produce stochastic dips and complex absorption at all energies (Hagino et al. 2016).

Hagino et al. (2016) model the hot phase of the wind, and include cool clumps in a phenomenological way to show that lines of sight which intercept the wind always show deep absorption features at iron from the hot, highly ionized phase of the wind, together with stochastic dips and complex absorption when the less ionized clumps occult the X-ray source. This model can give as good a fit as relativistic reflection to all the 2–30 keV data (*XMM–Newton* and NuSTAR) from 1H0707, and does not require a high-spin black hole (Hagino et al. 2016). This is rather different to the single ionization wind model, which still requires a contribution from highly relativistically smeared reflection (Dauser et al. 2012).

The clumpy wind absorption model also has the potential to explain the short reverberation lags observed. Gardner & Done (2015) show how a low spin, full spectral-timing model designed to explain the 200 s soft lag seen in PG1244 (Gardner & Done 2014a) can also match the lag-frequency data from 1H0707 just by including occultations. In their non-relativistic analysis, the occultation time-scale is simply the time taken for the clump to cover the source. This is $\Delta t \sim x R_{\rm g}\sqrt{r}/c$ for a source of size $xR_{\rm g}$, covered by a cloud on a circular orbit at $rR_{\rm g}$ of size scale larger than the source. The deep dips in 1H0707 take ∼200s (Fabian et al. 2012), so this would imply $x\sqrt{r} = 20$ or clumps orbiting at $r = 11$ for a source size of $6R_{\rm g}$ and a black hole mass of $2 \times 10^6\,{\rm M}_\odot$. It remains to be seen whether the clumpy winds which are generically produced from super Eddington flows (e.g. Takeuchi et al. 2014) can match these properties.

Similarly, it remains to be seen whether occultations can match the spectral behaviour, both during the dips (time-resolved spectra) and the high-frequency lag-energy (Fourier-resolved) spectra. The rather simple model of occulting clouds in Gardner & Done (2015) did not give a good fit to the dip spectra from 1H0707, but this model did not include reflection from the complex material on the far side of the source, and their clumps were highly ionized and single phase, rather than low ionization material embedded in a more highly ionized wind (see the sketch of the proposed geometry in Fig. 3). The high-frequency lag-energy spectra also contain features around the iron line energy, and again these require a simulation of the lag-energy spectrum expected from the full geometry of Fig. 3 in order to see whether this can match the data. We note that the lamppost model itself cannot easily match the high-frequency lag-energy spectra seen in 1H0707 (Kara et al. 2013; Wilkins et al. 2016), showing that the source geometry is almost certainly more complex.

One objection to the idea of cool clumps providing some of the variability in 1H0707 is that they will produce an iron fluorescence line if the clumps subtend a reasonable solid angle to the X-ray source. The line is smeared by the velocity structure of the wind, but without extreme relativistic effects it should be observable as a distinct feature rather than broadened into the red wing (Zoghbi et al. 2010). However, if the clumps are embedded in a more highly ionized wind, then Compton scattering in the highly ionized phase will reduce the observed line flux. Proper simulations of this geometry are clearly required in order to test whether the predicted line can indeed match the observed spectra from 1H0707.

5.2 The difference between simple and complex NLS1

The wind model sketched above gives a potential geometric explanation for the large difference in X-ray spectral behaviour between simple and complex NLS1. This difference must have its origin in a difference in one of the parameters which can affect the appearance of the black hole accretion flow, but several sources are seen to transition between simple and complex behaviour (Gallo 2006). Thus, the difference cannot originate with a fixed parameter such as spin. Instead, it must be associated with something which can vary. Fig. 3 clearly shows that inclination angle with respect to the wind can make a large difference in the observed properties of the inner X-ray source. Numerical simulations show that the polar and opening angle of the wind can fluctuate stochastically, as well as vary with $L/L_{\rm Edd}$, so the inclination angle with respect to the wind could be the required parameter determining the difference between simple and complex NLS1.

1H0707 (complex NLS1) and PG1244 (simple NLS1) have very similar Hβ linewidths and optical luminosity, and so have similar mass and mass accretion rates to zeroth order, and their masses are most probably low just from X-ray variability time-scale arguments. If 1H0707 is at higher inclination than PG1244 then it should have higher $L/L_{\rm Edd}$ for the same black hole spin. We take as an example 1H0707 at 60° and PG1244 at 30°, both with low spin and mass of $2 \times 10^6\,{\rm M}_\odot$. The colour (non-colour) temperature corrected discs give a mass accretion rates of 44(31)× Eddington for 1H0707 and 13(9) for PG1244, so both are still highly super-Eddington, but 1H0707 is more extreme than PG1244, as required by the optical spectra shown in Fig. 1, where 1H0707 lacks the narrow [O III] emission lines. Weak narrow lines are a characteristic of low ionization Broad Absorption Line quasars (Boroson & Meyers 1992), where this is likely due to shielding of the narrow line region by obscuration in a wind (see also Leighly 2004).

If 1H0707 is accreting at a higher Eddington ratio, this should also affect other features of the spectrum. $L/L_{\rm Edd}$ is known to affect the ratio of equivalent widths of emission lines in the broad line region, particularly Fe II/(broad) Hβ (Ferland et al. 2009). The iron blends shown for both NLS1 in Fig. 1 are quite similar, and similar also in terms of their ratio of Fe II/broad Hβ. If the correlation continues at these high $L/L_{\rm Edd}$ then 1H0707 should have a slightly lower iron abundance to PG1244 in order to produce the same ratio of Fe II/broad Hβ. However, it seems likely that the Fe II/Hβ ratio would also be affected by geometry of the wind, so the stronger wind in a more highly super-Eddington flow in 1H0707 could compensate for this.

Eddington ratio is also known to correlate strongly with the 2–10 keV spectral index (Shemmer et al. 2006; Vasudevan & Fabian 2007, 2009; Jin et al. 2012b). 1H0707 should then have a higher Γ than PG1244, though this is poorly constrained from spectral fits. Simple wind models fit to 1H0707 give $\Gamma = 3.5 \pm 0.8$ (Done et al. 2007), while more complex wind models are consistent with $\Gamma = 2.6$ (Hagino et al. 2016), whereas PG1244 has $\Gamma \sim 2.5$ (J13). Hence the data are consistent with a steeper index in 1H0707 as expected if it does have a higher $L/L_{\rm Edd}$, but do not significantly require this.

Thus, there is no obvious inconsistency with a model for these two NLS1 where they have similar low masses and spins but where 1H0707 has higher inclination, and hence its similar optical flux requires higher mass accretion rate. Both are super-Eddington, but 1H0707 is more super-Eddington than PG1244, so has a stronger wind which explains its lack of narrow optical line emission by shielding the NLR, suppressing the narrow [O III] lines compared to PG1244 (Leighly 2004). The combination of more highly super-Eddington flow leading to stronger mass loss together with higher inclination angle means that the wind is more likely to be in the line of sight for 1H0707.

This interpretation has much less soft X-ray emission than the low-mass, high-spin models required by the relativistic reflection interpretation. Nonetheless, the observed soft X-ray flux is still a factor of 90(11) times larger than the maximum observed from 1H0707, and 18(1.0) times than observed in PG1244. Thus, there is still a strong requirement of energy loss from the inner disc in 1H0707 and probably in PG1244 also. Strong energy losses are easily accommodated within the super-Eddington flows, as they can advect some of the power, and/or use it to launch a wind. It could also potentially launch an accretion powered jet, but both 1H0707 and PG1244 are very radio quiet, so substantial jet losses seem unlikely. A similarly extreme SED shape, with large advection/wind losses, is seen in one of the lowest mass AGN in the local Universe, GH08 (aka RX J1140.1+0307: Miniutti et al. 2009; Jin, Done & Ward 2016). A low spin solution requires less extreme energy loss, but this still over-predicts the observed 0.3–2 keV luminosity by a factor of $\geq$11 for the low-mass/high-inclination solution for 1H0707, even with no colour temperature correction.

5.3 Spin and the trigger for highly relativistic jets

Highly relativistic jets are the most dramatic pointer to an accreting black hole. Apparently, superluminal radio blobs can be explained only if the bulk Lorentz factor, Γ, is high, and if the angle, θ, between this motion and the observer's line of sight is small. The intrinsic emission of the blob is blue-shifted by a factor of δ and brightened by a factor of $\sim\delta^4$, so the jet emission from the core appears much more luminous in aligned versus non-aligned objects. This means that they are extremely bright in radio (synchrotron from the jet) and also in high-energy GeV gamma-rays (synchrotron self-Compton or External Compton from the jet; e.g. Ghisellini et al. 2010).

Another pointer to such relativistic jets is the radio lobe emission on much larger (kpc) scales. This is the interaction of the jet with its (stationary) environment, so is easily visible in non-aligned objects. Population studies show that the Fanaroff–Riely type I and II galaxies are consistent with being the misaligned versions of the highly beamed BL Lacs and Flat Spectrum Radio Quasars, respectively (Urry & Padovani 1995).

Most AGN do not show such large-scale radio structures, but weak core radio emission is ubiquitous. Clearly, the radio luminosity can also be dependent on the accretion power, so a better way to parametrize the importance of the radio jet is via the radio-loudness parameter, $\mathcal{R}$, defined as the ratio of flux at 5 GHz to that in the optical B band. This ratio changes by more than a factor of 1000, even when restricted to black holes of the same mass (Mclure & Jarvis 2004), or to black holes of the same $L/L_{\rm Edd}$ (Sikora, Stawasz & Lasota 2007). Clearly, it is very important to understand the origin of this spread in radio power, not only to understand relativistic jets but also to track their impact on their host galaxy via jet mode feedback.

Black hole binaries give some insight into the origin of this spread. These show a dramatic transition in their accretion flow properties at Eddington-scaled mass accretion rates $L/L_{\rm Edd} \leq 0.01$. This most probably marks the transition from a geometrically thin disc at high-mass accretion rates (Shakura & Sunyaev 1973) to a radiatively inefficient flow [advection dominated accretion flows (ADAF) Narayan & Yi 1995; Esin, McClintock & Narayan 1997], see e.g. the review by Done et al. (2007). This change in accretion

mode is strongly correlated with radio jet properties in the black hole binaries, with a steady, compact jet seen at low luminosities, which collapses, often by ejection of discrete blobs, when the flow makes a transition to a thin disc (Fender, Belloni & Gallo 2004). Thus, a single black hole binary can make a transition from being radio loud to radio quiet (Maccarone, Gallo & Fender 2003). However, none of this radio emission is ever associated with a highly relativistic outflow. Even the ejected blobs have speeds which are only mildly relativistic, at $\Gamma < 2$ (Gallo, Fender & Pooley 2003), while the similarities of the radio–X-ray correlation seen in binaries with very different inclinations show that the steady compact jet has $\Gamma \leq 1.7$ (Gallo et al. 2003). Similarly, the ubiquitous radio emission in radio-quiet AGN is also not from a highly relativistic jet, as it has comparable properties in both high and low inclination sources (Seyfert 2 and Seyfert 1s; Thean et al. 2001).

Thus, the radio emission seen in 'radio-quiet' AGN is mostly from an outflow which is not highly relativistic, but this does not in itself rule out a highly relativistic jet being present in all objects, perhaps forming a spine within a much slower outer sheath, as is also required in the blazars (Chiaberge et al. 2000, 2005; Ghisellini, Tavecchio & Chiaberge 2005). However, a BL Lac type spine emerging from every AGN with $L/L_{\rm Edd} < 0.01$ is inconsistent with the statistics of the GeV detections of AGN. The spine is highly beamed, so is aligned in only one out of $\Gamma^2 = 225$ AGN, and the spine jet should scale with accretion power (Heinz & Sunyaev 2003). Nonetheless, the resulting aligned jet is bright enough and the numbers of low-luminosity AGN are large enough that this over-predicts the observed *Fermi* All Sky Survey numbers of BL Lacs by a factor of 1000 (Gardner & Done 2014b).

Current consensus is that all jets are probably powered by a combination of rotation and magnetic field, but there are two main models for their formation, either using the rotational energy of the black hole (Blandford & Znajek 1977, hereafter BZ, or spin powered jet), or the accretion flow (Blandford & Payne 1982, hereafter BP, or accretion powered jet). High black hole spin producing a spin-powered jet has long been identified as the possible trigger for launching and powering the most highly relativistic jets (BZ; Begelman, Blandford & Rees 1984; Wilson & Colbert 1995). This is supported by recent numerical simulations of the accretion flow which show that truly relativistic outflows are produced predominantly by spin power, while lower velocity outflows are driven by a combination of BP and other mechanisms (see e.g. the review by Yuan & Narayan 2014).

There are two types of jets in theory and numerical simulations, one highly relativistic and another not so highly relativistic , and two types of jets seen in observations, one highly relativistic and another not so highly relativistic. It is clearly inherently a very attractive idea to associate the highly relativistic jets with BZ and hence high-spin black holes, and the rest to low spin black holes producing only accretion-powered outflows (e.g. Maraschi et al. 2012). The only reason this very attractive idea was dropped was the observational evidence for high black hole spin in radio-quiet objects (Ghisellini, Haardt & Matt 2004). However, the majority of high-spin measurements of radio-quiet objects are for complex NLS1 such as 1H0707 (see e.g. the compilation of Reynolds 2013). If these other NLS1 are likewise super-Eddington, as claimed by Collin & Kawaguchi (2004), then these also have inner discs which are unlikely to be flat, inconsistent with the lamppost/flat disc geometry used to derive the high-spin values. If these high-spin values are not robust then this removes the argument against the simplest models of jets, whereby a low Lorentz factor accretion powered jet is present in all sources, though its structure and power depend on the accretion flow configuration, with a spin powered jet only in the highest spin objects, again with its structure and power depending on the accretion flow configuration. High spin can then be a necessary and sufficient condition for a highly relativistic jet.

If instead the 'complex' NLS1 do indeed have high spin, then the trigger for highly relativistic jets must instead be some additional, external parameter such as accretion of magnetic flux from the halo (Sikora & Begelman 2013). Such models have no predictive power, which limits the confidence with which the jet mode feedback can be modelled in cosmological simulations of the growth of large-scale structure in the Universe (e.g. Bower et al. 2006).

6 CONCLUSIONS

Both 1H0707 and PG1244 have optical/UV spectra which clearly require super-Eddington mass accretion rates through their outer disc. However, these over-predict the observed bolometric luminosities so there must also be advective and/or kinetic losses. The inner accretion disc is then not at all likely to be flat, as assumed in the lamppost models, with a smooth shape produced by pure advection losses but with an additional clumpy turbulent wind produced in the numerical simulations. Any such vertical structure on the disc means that inclination angle is important, and can dramatically alter our view of the central regions. We suggest that this is the origin of the distinction between 'simple' and 'complex' NLS1, with the characteristic deep X-ray intensity dips seen in the 'complex' NLS1 being produced by occultation of the central source by the upper edge of the vertical structure.

We speculate that this may allow low spin models for the 'complex' NLS1, in which case high black hole spin may be a necessary and sufficient condition required to produce highly relativistic jets.

ACKNOWLEDGEMENTS

CD thanks Karen Leighly for the CTIO optical spectral data of 1H0707 shown in Fig. 1, and Xinlin Zhou for some earlier work on the X-ray spectra of 1H0707. CD acknowledges STFC funding under grant ST/L00075X/1. Funding for SDSS-III has been provided by the Alfred P. Sloan Foundation, the Participating Institutions, the National Science Foundation, and the U.S. Department of Energy Office of Science. The SDSS-III web site is http://www.sdss3.org/. This work is based on observations obtained with *XMM–Newton*, an ESA science mission with instruments and contributions directly funded by ESA Member States and the USA (NASA). All data used in this paper are publicly available in the archives. We thank the referee for their comments, which considerably improved the paper. CD acknowledges STFC funding under grant ST/L00075X/1 All comments/changes are here rather than on the pdf of the paper.

REFERENCES

Ai Y. L., Yuan W., Zhou H., Wang T. G., Dong X.-B., Wang J. G., Lu H. L., 2013, AJ, 145, 90
Alston W. N., Done C., Vaughan S., 2014, MNRAS, 439, 1548
Baskin A., Laor A., Stern J., 2014a, MNRAS, 438, 604
Baskin A., Laor A., Stern J., 2014b, MNRAS, 445, 3025
Begelman M. C., Blandford R. D., Rees M. J., 1984, Rev. Modern Phys., 56, 255
Bessell M. S., 1991, A&A, 242, L17
Blandford R. D., Payne D. G., 1982, MNRAS, 199, 883 (BP)
Blandford R. D., Znajek R. L., 1977, MNRAS, 179, 433 (BZ)
Boroson T. A., Meyers K. A., 1992, ApJ, 397, 442

Bower R. G., Benson A. J., Malbon R., Helly J. C., Frenk C. S., Baugh C. M., Cole S., Lacey C. G., 2006, MNRAS, 370, 645
Cackett E. M., Zoghbi A., Reynolds C., Fabian A. C., Kara E., Uttley P., Wilkins D. R., 2014, MNRAS, 438, 2980
Chiaberge M., Celotti A., Capetti A., Ghisellini G., 2000, A&A, 358, 104
Chiaberge M. et al., 2005, ApJ, 629, 100
Collin S., Kawaguchi T., 2004, A&A, 426, 797
Collin-Souffrin S., Joly M., Dumont S., Heidmann N., 1980, A&A, 83, 190
Dauser T. et al., 2012, MNRAS, 422, 1914
Davis S. W., Laor A., 2011, ApJ, 728, 98
Davis S. W., Woo J. H., Blaes O. M., 2007, ApJ, 668, 682
Done C., Gierliński M., Kubota A., 2007, A&AR, 15, 1
Done C., Sobolewska M. A., Gierliński M., Schurch N. J., 2007, MNRAS, 374, L15
Done C., Davis S. W., Jin C., Blaes O., Ward M., 2012, MNRAS, 420, 1848
Done C., Jin C., Middleton M., Ward M., 2013, MNRAS, 434, 1955 (D13)
Dovciak M., De Marco B., Kara E., Matt G., Karas V., Miniutti G., Alston W., 2014, The X-ray Universe 2014, Id. 244, available at: http://www.cosmos.esa.int/documents/332006/744654/MDovciak2_p.pdf
Ebisawa K., Mitsuda K., Hanawa T., 1991, ApJ, 367, 213
Esin A. A., McClintock J. E., Narayan R., 1997, ApJ, 489, 865
Fabian A. C., Rees M. J., Stella L., White N. E., 1989, MNRAS, 238, 729
Fabian A. C., Iwasawa K., Reynolds C. S., Young A. J., 2000, PASP, 112, 1145
Fabian A. C., Miniutti G., Gallo L., Boller Th., Tanaka Y., Vaughan S., Ross R. R., 2004, MNRAS, 353, 1071
Fabian A. C. et al., 2009, Nature, 459, 540
Fabian A. C. et al., 2012, MNRAS, 419, 116
Fender R. P., Belloni T. M., Gallo E., 2004, MNRAS, 355, 1105
Ferland G. J., Hu C., Wang J.-M., Baldwin J. A., Porter R. L., van Hoof P. A. M., Williams R. J. R., 2009, ApJ, 707, L82
Gallo L. C., 2006, MNRAS, 368, 479
Gallo E., Fender R. P., Pooley G. G., 2003, MNRAS, 344, 60
Gardner E., Done C., 2014a, MNRAS, 438, 779
Gardner E., Done C., 2014b, MNRAS, 442, 2456
Gardner E., Done C., 2015, MNRAS, 448, 2245
Ghisellini G., Haardt F., Matt G., 2004, A&A, 413, 535
Ghisellini G., Tavecchio F., Chiaberge M., 2005, A&A, 432, 401
Ghisellini G., Tavecchio F., Foschini L., Ghirlanda G., Maraschi L., Celotti A., 2010, MNRAS, 402, 497
Hagino K., Odaka H., Done C., Tomaru R., Watanabe S., Takahashi T., 2016, preprint (arXiv:1509.05645)
Heinz S., Sunyaev R. A., 2003, MNRAS, 343, L59
Hubeny I., Blaes O., Krolik J. H., Agol E., 2001, ApJ, 559, 680
Jin C., Ward M., Done C., Gelbord J., 2012a, MNRAS, 420, 1825
Jin C., Ward M., Done C., 2012b, MNRAS, 425, 907
Jin C., Done C., Middleton M., Ward M., 2013, MNRAS, 436, 3173 (J13)
Jin C., Done C., Ward M., 2016, MNRAS, 455, 691
Jones D. H. et al., 2009, MNRAS, 399, 683
Kalberla P. M. W., Burton W. B., Hartmann D., Arnal E. M., Bajaja E., Morras R., Pöppel W. G. L., 2005, A&A, 440, 775
Kara E., Fabian A. C., Cackett E. M., Steiner J. F., Uttley P., Wilkins D. R., Zoghbi A., 2013, MNRAS, 428, 2795
Kara E., Cackett E. M., Fabian A. C., Reynolds C., Uttley P., 2014, MNRAS, 439, L26
Kaspi S., Smith P. S., Netzer H., Maoz D., Jannuzi B. T., Giveon U., 2000, ApJ, 533, 631
Kelly B. C., Treu T., Malkan M., Pancoast A., Woo J. H., 2013, ApJ, 779, 187
Krolik J. H., McKee C. F., Tarter C. B., 1981, ApJ, 249, 422
Kubota A., Makishima K., Ebisawa K., 2001, ApJ, 560, L147
Laor A., Davis S. W., 2011, MNRAS, 417, 681
Leighly K. M., 1999, ApJS, 125, 29
Leighly K. M., 2004, ApJ, 611, 125
Leighly K. M., Moore J. R., 2004, ApJ, 611, L107
Maccarone T. J., Gallo E., Fender R., 2003, MNRAS, 345, L19
McLure R. J., Jarvis M. J., 2004, MNRAS, 353, L45
Maraschi L., Colpi M., Ghisellini G., Perego A., Tavecchio F., 2012, J. Phys. Conf. Ser., 355, 012016
Marconi A., Axon D. J., Maiolino R., Nagao T., Pastorini G., Pietrini P., Robinson A., Torricelli G., 2008, ApJ, 678, 693
Miller L., Turner T. J., Reeves J. N., George I. M., Kraemer S. B., Wingert B., 2007, A&A, 463, 131
Miller L., Turner T. J., Reeves J. N., Braito V., 2010, MNRAS, 408, 1928
Miniutti G., Fabian A. C., 2004, MNRAS, 349, 1435
Miniutti G., Ponti G., Greene J. E., Ho L. C., Fabian A. C., Iwasawa K., 2009, MNRAS, 394, 443
Mizumoto M., Ebisawa K., Sameshima H., 2014, PASJ, 66, 122
Narayan R., Yi I., 1995, ApJ, 452, 710
Ponti G., Papadakis I., Bianchi S., Guainazzi M., Matt G., Uttley P., Bonilla N. F., 2012, A&A, 542, A83
Reynolds C. S., 2013, Classical Quantum Gravity, 30, 244004
Robertson D., Gallo L. C., Zoghbi A., Fabian A. C., 2015, MNRAS, 453, 3455
Shakura N. I., Sunyaev R. A., 1973, A&A, 24, 337
Shemmer O., Brandt W. N., Netzer H., Maiolino R., Kaspi S., 2006, ApJ, 646, L29
Sikora M., Begelman M. C., 2013, ApJ, 764, L24
Sikora M., Stawarz Ł., Lasota J.-P., 2007, ApJ, 658, 815
Smith R., Vaughan S., 2007, MNRAS, 375, 1479
Takeuchi S., Ohsuga K., Mineshige S., 2014, PASJ, 66, 48
Thean A., Pedlar A., Kukula M. J., Baum S. A., O'Dea C. P., 2001, MNRAS, 325, 737
Urry C. M., Padovani P., 1995, PASP, 107, 803
Uttley P., Cackett E. M., Fabian A. C., Kara E., Wilkins D. R., 2014, A&AR, 22, 72
Vasudevan R. V., Fabian A. C., 2007, MNRAS, 381, 1235
Vasudevan R. V., Fabian A. C., 2009, MNRAS, 392, 1124
Vasudevan R., Gallo L., Robertson D., Fulford K., 2011, Proceedings of Science.Narrow-Line Seyfert 1 Galaxies and their Place in the Universe, Id. 7
Vestergaard M., Peterson B. M., 2006, ApJ, 641, 689
Wilkins D. R., Cackett E. M., Fabian A. C., Reynolds C. S., 2016, MNRAS, 458, 200
Wilson A. S., Colbert E. J. M., 1995, ApJ, 438, 62
Woo J., Urry C. M., 2002, ApJ, 579, 530
Yuan F., Narayan R., 2014, ARA&A, 52, 529
Zoghbi A., Fabian A. C., Uttley P., Miniutti G., Gallo L. C., Reynolds C. S., Miller J. M., Ponti G., 2010, MNRAS, 401, 2419
Zoghbi A., Uttley P., Fabian A. C., 2011, MNRAS, 412, 59

This paper has been typeset from a TEX/LATEX file prepared by the author.